Finite size effects on the light curves of slowly-rotating neutron stars

Hajime Sotani,[1,*] Hector O. Silva,[2,†] and George Pappas[3,4,‡]

[1]*Division of Science, National Astronomical Observatory of Japan, 2-21-1 Osawa, Mitaka, Tokyo 181-8588, Japan*

[2]*eXtreme Gravity Institute, Department of Physics, Montana State University, Bozeman, Montana 59717, USA*

[3]*Dipartimento di Fisica, "Sapienza" Universitá di Roma & Sezione INFN Roma1, Piazzale Aldo Moro 5, 00185, Roma, Italy*

[4]*Department of Physics, Aristotle University of Thessaloniki, Thessaloniki 54124, Greece*

(Received 23 May 2019; published 9 August 2019)

An important question when studying the light curves produced by hot spots on the surface of rotating neutron stars is, how might the shape of the light curve be affected by relaxing some of the simplifying assumptions that one would adopt on a first treatment of the problem, such as that of a pointlike spot. In this work we explore the dependence of light curves on the size and shape of a single hot spot on the surface of slowly rotating neutron stars. More specifically, we consider two different shapes for the hot spots (circular and annular) and examine the resulting light curves as functions of the opening angle of the hot spot (for both) and width (for the latter). We find that the pointlike approximation can describe light curves reasonably well, if the opening angle of the hot spot is less than ∼5°. Furthermore, we find that light curves from annular spots are almost the same as those of the full circular spot if the opening angle is less than ∼35° independently of the hot spot's width.

DOI: 10.1103/PhysRevD.100.043006

I. INTRODUCTION

Supernova explosions, the last act of massive stars, are the birth places of neutron stars. During these processes, the density inside the star significantly exceeds the standard nuclear density and the gravitational and magnetic fields inside/around the star become much stronger than those in the Solar System [1]. Thus, the resulting neutron stars are the best natural candidates for probing the physics under these extreme environments. In fact, due to the saturation property of nuclear matter, it is challenging to obtain information about matter in such high-density regions in Earth laboratories, which leads to many uncertainties in the equation of state (EOS) of neutron stars [2]. This difficulty may be overcome by observing neutron stars themselves and/or the phenomena associated to them. One of the main observational constraints on the EOS at supranuclear densities comes from the discoveries of $\sim 2M_\odot$ neutron stars [3–5]. Due to the existence of such massive neutron stars one can exclude the soft EOSs that have expected maximum masses that are less than the observed neutron star masses. Another constraint on the EOS is the information about the tidal deformability obtained from the observation of the gravitational waves emitted by GW170817, which is the binary neutron star merger [6,7]. From the obtained tidal deformability, the radius of a 1.4 $M_\odot$ neutron star is constrained to be around ≈11 km [8] with a maximum value of 13.6 km [9], which suggests that some of the relatively stiffer EOSs in the low density region should be ruled out. These examples demonstrate that the observations of neutron stars and astrophysical phenomena involving them are essential for constraining the EOS of neutron star matter at high densities [10].

Electromagnetic observations of astrophysical processes involving neutron stars offer another avenue to probe the properties of these extreme objects. Due to their strong gravitational field, radiation from the immediate vicinity of neutron stars experiences gravitational light bending, the magnitude of which is controlled by the star's mass and radius, allowing (in principle) these parameters to be inferred and consequently be used to shed light on the underlying EOS [11–14]. Prime systems for such studies include accreting millisecond pulsars and x-ray bursters. In both scenarios, parts of the star's surface are heated, producing in this way hot spots (relative to the rest of the star). These hot spots corotate with the star producing an observable x-ray flux which is modulated by the star's spin frequency, called a light curve (or pulse profile). These light curves encode information about the physical properties

*sotani@yukawa.kyoto-u.ac.jp
†hector.okadadasilva@montana.edu
‡gpappas@auth.gr

 © 2019 American Physical Society

of the hot spot such as e.g., its size, geometry, temperature distribution and spectra. Moreover, they encode information of the spacetime curvature around the star and thereby of the bulk properties of the star. One of the main goals of the ongoing Neutron star Interior Composition ExploreR (NICER) [15–17] mission is to measure light curves from a number of sources with unprecedented time resolution, constraining their masses and radii within 5%–10% accuracy in optimal cases [18–20] (see also e.g., [21–23]).

Several theoretical studies of the properties of light curves from hot spots on the surface of rotating neutron stars have been carried out in the past (see e.g., [24–28]). The contribution of the various ingredients that affect the shape of a light curve due to the rotation of the neutron star have been studied in several instances. For example, there have been calculations of the light curve that are taking into account the Doppler factor and the time delay in the Schwarzschild spacetime [26,29–31].[1] In other cases, light curves were calculated either within the Hartle-Thorne approximation [32] or in the numerically determined spacetime of rapidly rotating neutron stars [33,34]. These works showed that the inclusion of effects such as Doppler, aberration and gravitational time delay in the Schwarzschild spacetime can estimate relatively well the light curve produced by moderately rapidly rotating neutron stars with spin frequencies $\lesssim$300 Hz, above which the inclusion of stellar oblateness is required [33–36]. In addition, since light curves from neutron stars also depend on the spacetime geometry and on the gravitational theory, one can use light curve observations to perform strong-field tests of general relativity (GR), although the effect of the gravitational theory may be degenerate with uncertainties on the EOS [37–40].

A simplifying assumption used in some of these studies is that of a pointlike approximation for the hot spot, where its size is assumed to be negligible. This approximation may be valid under some conditions, but in realistic astrophysical scenarios one should take into account the finite-size effects of the hot spot on the light curve (e.g., [41,42]). Furthermore, hydromagnetic numerical simulations of accreting millisecond pulsars reveal that these hot spots might not necessarily even be circular and can instead have ring or crescent-moonlike shapes [43,44] with implications on the resulting light curve of known systems [45,46].

In this work, we examine in detail the effects of the shape and size of single hot spots, in the controlled scenario of slowly rotating neutron stars, which allows one to single out their effects in the light curve. This paper is organized as follows. In Sec. II we summarize the theory behind light curve modeling of slowly rotating neutron stars, with special emphasis on how to deal with finite-size effects of the hot spot. In Sec. III we discuss how these light curves are calculated numerically and present a simple approach to study ring-shaped hot spots. Then, we investigate in detail the resulting light curves, considering different hot-spot-observer arrangements and hot spot sizes. We also contrast the differences between circular and annular hot spots and in the latter case examine the validity of the pointlike hot spot approximation. Finally, in Sec. IV we summarize our findings and discuss possible extensions of our work. We use geometric units, $c = G = 1$, where c and G denote the speed of light in vacuum and the gravitational constant respectively, and use metric signature $(-,+,+,+)$.

II. RADIATION FLUX FROM SLOWLY ROTATING NEUTRON STARS

For generality, we consider the following line element for a static, spherically symmetric spacetime given by

$$ds^2 = -A(r)dt^2 + B(r)dr^2 + C(r)(d\theta^2 + \sin^2\theta d\psi^2), \quad (1)$$

where we focus on asymptotically flat spacetimes for which $A(r) \to 1$, $B(r) \to 1$, and $C(r) \to r^2$ as $r \to \infty$. In these coordinates, the circumference radius, r_c, is given by $r_c^2 \equiv C(r)$ at each radial position r. This line element is general enough to describe neutron stars not only in GR, but also in modified theories of gravity [37,39]. While in Sec. III the particular case of the Schwarzschild spacetime is taken, in the present section we develop a general approach for dealing with finite sized hot spots that can readily be used outside of GR.

Let us consider the trajectory of photons on this spacetime, initially emitted from the star's surface located at $r = R$ and propagating outwards to an observer located at a distance D ($\gg R$) from the star. The equation of motion for null geodesics can be obtained from the Euler-Lagrange equation, i.e.,

$$\frac{\partial \mathcal{L}}{\partial x^\mu} - \frac{d}{d\lambda}\left(\frac{\partial \mathcal{L}}{\partial \dot{x}^\mu}\right) = 0, \quad (2)$$

where $\mathcal{L}$ is the Lagrangian and the dot denotes a derivative with respect to an affine parameter λ. Using Eq. (1), we obtain

$$2\mathcal{L} = -A\dot{t}^2 + B\dot{r}^2 + C\dot{\psi}^2, \quad (3)$$

where, due to spherical symmetry, we can choose the photon trajectory to be on the plane $\theta = \pi/2$ without loss of generality. Then, combining Eqs. (2) and (3), the angle at the stellar surface $\psi(R)$ is given by [24]

$$\psi(R) = \int_R^\infty \frac{dr}{C}\left[\frac{1}{AB}\left(\frac{1}{b^2} - \frac{A}{C}\right)\right]^{-1/2}, \quad (4)$$

[1]The slow-rotating approximation without the Doppler factor and the time delay is valid at least with ~0.1 Hz [31], while one can see the significant deviation with a few hundred Hz [26,30].

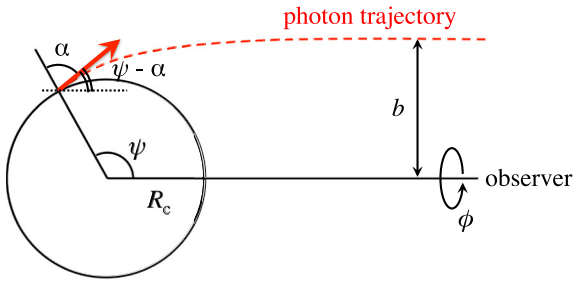

FIG. 1. Geometry used to describe the emission of photons from a neutron star. The dashed line indicates the trajectory of a photon, emitted with an angle α (measured with respect to the normal to the star's surface) from the star's surface R_c [$R_c = C^{1/2}(R)$] from a point located at ψ (measured with respect to the line of sight to the observer). The star's gravitational field bends the trajectory by an amount $\psi - \alpha$ and the photon is observed arriving with an impact parameter b. The angle ϕ denotes the azimuthal angle in the observer's sky.

where

$$\sin\alpha = b\sqrt{\frac{A(R)}{C(R)}}, \tag{5}$$

with $b \equiv \ell/e$ being the impact parameter, defined in terms of the photon's energy e and angular momentum ℓ, while α is the emission angle as shown in Fig. 1, measured relative to the normal to the star's surface.

Using Eqs. (4) and (5), we can numerically calculate the relation between $\psi(R)$ and α for a given radius R (once A, B and C have been specified), where the value of ψ increases as α increases. This allows us to define a critical value of ψ,

$$\psi_{\rm cri} \equiv \psi(\alpha = \pi/2), \tag{6}$$

for a photon to reach the observer, where $\alpha = \pi/2$ means that the photon is emitted tangentially with respect to the stellar surface. This in turn allows us to introduce the notion of an *invisible zone*, defined by $\alpha > \pi/2$ (or $\psi > \psi_{\rm cri}$) wherein photons cannot reach the observer. We remark that the $\psi_{\rm cri}$ (and thus the invisible zone) also depends on the underlying theory of gravity.

Since light bending is a GR effect, $\psi_{\rm cri}$ increases as the gravitational field becomes stronger. Thus, the value of $\psi_{\rm cri}$ increases (or conversely, the invisible zone decreases) as the compactness $\mathcal{C} \equiv M/R$ of the radiating object increases. In the Schwarzschild spacetime, the invisible zone vanishes if $\mathcal{C} \geq 0.284$, implying that the whole surface of the star is visible to the observer. In the absence of an invisible zone, photon trajectories can whirl around the star multiple times [24,47] resulting in multiple images of the star's surface. These strong lensing effects do not happen for canonical neutron stars for which $M/R \lesssim 0.2$ (see Fig. 3 in Ref. [47]), which we consider hereafter.

How do we calculate the flux measured by an observer, that is coming from a single hot spot on the star's surface? The area of the hot spot, dS, and the corresponding solid angle on the observer's sky, $d\Omega$, are given by

$$dS = C(R)\sin\psi d\psi d\phi, \tag{7}$$

$$d\Omega = \frac{b db d\phi}{D^2}, \tag{8}$$

where, recall, D is the distance between the star and the observer, while ϕ is an azimuthal angle in the observer's sky as shown in Fig. 1. The observed spectral flux, dF_E, inside $d\Omega$ is expressed as

$$dF_E = I_E d\Omega, \tag{9}$$

where I_E is the specific intensity of the radiation measured in terms of the energy E measured at infinity by the observer. It is however more convenient to write I_E in terms of the specific intensity $I_0(E_0, \alpha)$ measured by an observer at the vicinity of the stellar surface. These two specific intensities are related as

$$I_E = A(R)^{3/2} I_0(E_0, \alpha), \tag{10}$$

where E_0 is the photon energy measured by an observer at the vicinity of the star's surface.

We can now combine Eq. (10) with Eqs. (5), (8), and (9) to obtain

$$dF_E = \frac{A(R)^{1/2}C(R)}{D^2} I_0(E_0, \alpha)\sin\alpha\cos\alpha\frac{d\alpha}{d\psi}d\psi d\phi, \tag{11}$$

which, upon integration over all energies E, leads to the observed bolometric flux dF,

$$\begin{aligned} dF &= \int_0^\infty dF_E dE, \\ &= \frac{A(R)C(R)}{D^2} I_0(\alpha)\sin\alpha\cos\alpha\frac{d\alpha}{d\psi}d\psi d\phi. \end{aligned} \tag{12}$$

Here, $I_0(\alpha) \equiv \int I_0(E_0, \alpha) dE_0$ is the bolometric intensity measured in the vicinity of the stellar surface. To derive Eq. (12) we also converted the emitted to observed energies using the usual redshift relation

$$E = A(R)^{1/2} E_0. \tag{13}$$

Although I_0 generally depends on the emission angle due to scattering as photons propagate through the neutron star's atmosphere [48–51], we consider for simplicity that the emission is uniform, i.e., $I_0 = $ const., as in the previous studies (e.g., [27,31,37]). The bolometric flux F and the observed area of the hot spot S are then given by

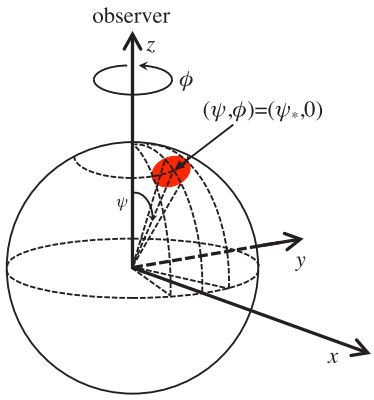

FIG. 2. At any time, one can choose the coordinate where the center of the hot spot is located at $(\psi, \phi) = (\psi_*, 0)$.

$$F = F_1 \iint_S \sin\alpha \cos\alpha \frac{d\alpha}{d\psi} d\psi d\phi,$$
$$S = C(R) \iint_S \sin\psi d\psi d\phi, \tag{14}$$

with

$$F_1 \equiv \frac{I_0 A(R) C(R)}{D^2}, \tag{15}$$

and where $\iint_S$ means that the integration should be done only over the region occupied by the hot spot.

Let us consider the case where the hot spot is circular, with size determined by an opening angle $\Delta\psi$. As shown in Fig. 2, we can choose the coordinate at any time, where the center of the hot spot is located at $(\psi, \phi) = (\psi_*, 0)$. In these coordinates, the unit vector pointing to the center of the hot spot, $\boldsymbol{n}$, and the unit vector pointing to an arbitrary position of (ψ, ϕ), $\boldsymbol{x}$, are given by $\boldsymbol{n} = (\sin\psi_*, 0, \cos\psi_*)$ and $\boldsymbol{x} = (\sin\psi\cos\phi, \sin\psi\sin\phi, \cos\psi)$. The condition that the position of (ψ, ϕ) is inside the circular hot spot is $\cos(\Delta\psi) \leq \boldsymbol{n} \cdot \boldsymbol{x}$, which yields

$$\cos(\Delta\psi) \leq \sin\psi_* \sin\psi \cos\phi + \cos\psi_* \cos\psi. \tag{16}$$

The hot spot on a rotating neutron star with an angular velocity ω measured by the observer is characterized by two angles, i and Θ, as shown in Fig. 3. That is, Θ is the angle between the center of the hot spot and the rotation axis, while i is the angle between the direction to the observer and the rotation axis. Choosing $t = 0$ when the hot spot is closest to the observer, the angular position of the center of the hot spot, ψ_*, is given by

$$\cos\psi_* = \sin i \sin\Theta \cos(\omega t) + \cos i \cos\Theta. \tag{17}$$

Within the pointlike approximation ($\Delta\psi \approx 0$) (see the top panel of Fig. 4) one can classify when the hot spot would be visible as a function of the angles of i and Θ, as a function of $\psi_{\rm cri}$ as follows [30]:

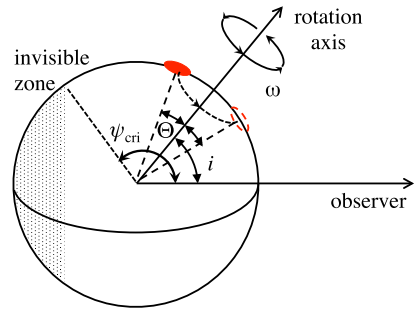

FIG. 3. Illustration of the hot spot on a rotating star with angular velocity ω. The angle between the direction to the observer and the rotation axis is i, while the angle between the center of the hot spot and the rotation axis is Θ. The shaded region denotes the invisible zone whose boundary is determined by the angle $\psi_{\rm cri}$.

(i) region A: the hot spot is always observed,
(ii) region B: the hot spot enters the invisible zone for a fraction of the period,
(iii) region C: the hot spot is invisible at any time.

When we include a finite size to the hot spot the boundaries between these regions become blurred, as illustrated in the bottom panel of Fig. 4. In this panel, the shaded region corresponds to the situation in which a part of the hot spot can enter the invisible zone.

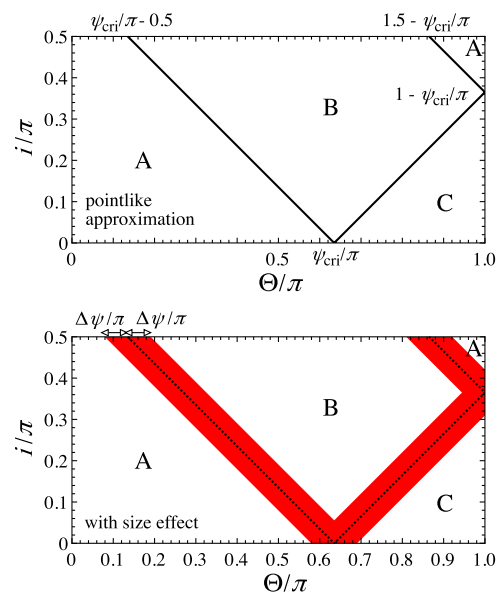

FIG. 4. Visibility classification of the single hot spot, as a function of the angles of i and Θ. The top panel corresponds to the case with a pointlike approximation, where three situations exist, i.e., (A) the hot spot can be always observed, (B) the hot spot can enter the invisible zone for a fraction of the period, and (C) the hot spot cannot be observed in any time. The bottom panel corresponds to the case with the effect of hot spot size, where the boundary of the classification becomes blurred. This example is the case for $\Delta\psi = 10°$. The colored region denotes the situation that a part of the hot spot can enter the invisible zone.

III. LIGHT CURVES OF FINITE-SIZED HOT SPOTS

Until this point, our discussion has been very general and applicable for a wide family of spacetimes whose line element can be written in the form (1). From now on, we consider the particular case of the Schwarzschild spacetime to describe the star's exterior spacetime (motivated by Birkhoff's theorem in GR) for which

$$A(r) = 1 - \frac{2M}{r}, \quad B(r) = \frac{1}{A(r)}, \quad C(r) = r^2. \tag{18}$$

Nonetheless, we emphasize that the calculations and methods present here can be applied to other static, spherically symmetric spacetimes.

Furthermore, to focus our attention on how the spot's area affects the light curve, we consider for simplicity only slowly rotating neutron stars, where one can neglect the rotational effects, such as Doppler shifts, aberration and the time delay [29–31]. In this case, the light curve obtained for $(\Theta, i) = (a, b)$ is the same as that obtained for $(\Theta, i) = (b, a)$, a symmetry that arises due to Eq. (17). In practice, we analyze light curves only for $\Theta = i$ and more specifically show representative results for the cases with $\Theta = i = 30°$, 45°, 60°, and 90°. An additional symmetry of the light curve is that its amplitude at t/T for $0.5 \leq t/T \leq 1$ is the same as that at $1 - t/T$, where T is the rotational period defined by $T \equiv 2\pi/\omega$. In light of these properties, we limit our calculation of the light curves in the rotation phase interval $0 \leq t/T \leq 0.5$. For our stellar models, we consider two stars with $R = 5M$ and $4M$, for which $\psi_{\rm cri}$ are respectively $\psi_{\rm cri} = 0.7191\pi$ (129.4°) and $\psi_{\rm cri} = 0.8476\pi$ (152.6°).

Considering these models, we further assume two possible geometries for the hot spot. First, in Sec. III A, we consider circular hot spots with an opening angle $\Delta\psi$, as shown in the left-hand-side of Fig. 5. Next, in Sec. III B, we study hot spots with an annular shape. This geometry is obtained by removing from an otherwise circurlar hot spot (with angular radius $\Delta\psi$) an internal circular region with opening angle $\Delta\psi_i$. This situation is illustrated in the right-hand side of Fig. 5. In both cases, the hot spot's center is fixed at $\psi = \psi_*$.

To calculate the light curve of a circular hot spot we proceed as follows. For any time instant, the center of the spot ψ_* is determined from Eq. (17). Since the flux with a specific value of ψ is independent of the value of ϕ, the flux from the hot spot is calculated from Eq. (14) as

$$F(\Delta\psi) = 2F_1 \int_{\psi_*-\Delta\psi}^{\psi_*+\Delta\psi} \phi(\psi) \sin\alpha \cos\alpha \frac{d\alpha}{d\psi} d\psi, \tag{19}$$

where $\phi(\psi)$ is the boundary of the hot spot in the ϕ direction determined from the constraint equation (16) as a function of ψ. As we explained previously, we can determine $\alpha(\psi)$ using Eqs. (4) and (5), once a mass M and radius R have been specified for the neutron star.

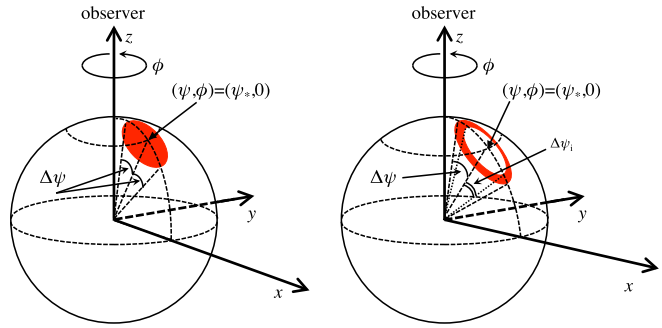

FIG. 5. Illustration of two different geometries for the hot spot. Left image: a circular hot spot with angular radius $\Delta\psi$. Right image: an annular geometry with width $\Delta\psi - \Delta\psi_i$. In both cases, the center of the hot spot is chosen to be $\psi = \psi_*$.

In the case of an annular hot spot we exploit our assumptions of isotropic emission and slow rotation. Under these assumptions, the flux coming from the excised internal region (centered at ψ_* with opening angle $\Delta\psi_i$) can simply be *subtracted* from the flux of the total circular spot of opening angle $\Delta\psi$, i.e.,

$$\begin{aligned} F &= F(\Delta\psi) - F(\Delta\psi_i) \\ &= 2F_1 \int_{\psi_*-\Delta\psi}^{\psi_*+\Delta\psi} \phi(\psi) \sin\alpha \cos\alpha \frac{d\alpha}{d\psi} d\psi \\ &\quad - 2F_1 \int_{\psi_*-\Delta\psi_i}^{\psi_*+\Delta\psi_i} \phi_i(\psi) \sin\alpha \cos\alpha \frac{d\alpha}{d\psi} d\psi, \end{aligned} \tag{20}$$

where $\phi_i(\psi)$ is the boundary of the inner circle.

A. Circular hot spots

First, let us consider the light curves with the filled circle hot spots, as shown in the left-hand side of Fig. 5. In the top panels of Fig. 6, we show the light curves for the neutron star model with $R = 5M$, where the different lines correspond to the results with different values of $\Delta\psi$ and for reference the results with the pointlike approximation are also shown by the open circles. The panels from left to right correspond the results for the cases with $i = \Theta = 30°$, 45°, 60°, and 90°. To make explicit the role of the hot spot size on the light curve relative to those calculated in the pointlike approximation, we show the relative deviation defined as

$$\Delta \equiv \frac{|F/F_{\rm max} - F^{(\rm p)}/F^{(\rm p)}_{\rm max}|}{F/F_{\rm max}} \tag{21}$$

in the bottom panels of Fig. 6. In Eq. (21), $F/F_{\rm max}$ and $F^{(\rm p)}/F^{(\rm p)}_{\rm max}$ denote respectively the observed bolometric fluxes normalized by the maximum flux including the effect of the spot's finite size and that calculated using the

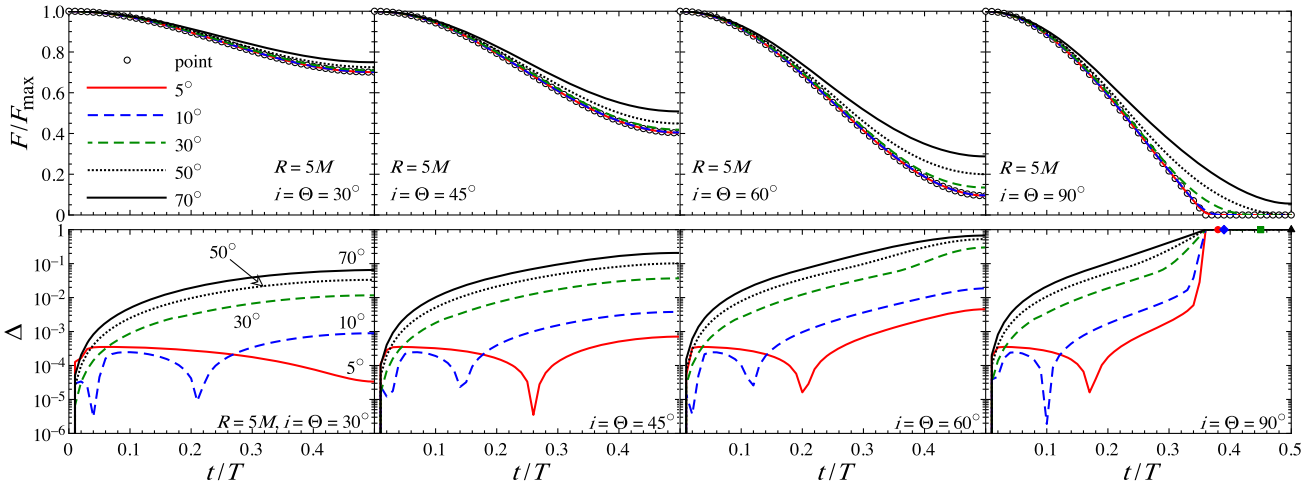

FIG. 6. For the neutron star model with $R = 5M$, the light curves calculated considering the finite area of the hot spot are compared with that with the pointlike spot approximation. In the top panels, the light curves with various opening angle ($\Delta\psi = 5°$, 10°, 30°, 50°, and 70°) are shown with different lines, while the light curves with the pointlike approximation are shown with the open circles, where the all light curves are normalized by their maximum values, i.e., the flux at $t/T = 0$. In the bottom panels, the relative deviations calculated by Eq. (21) are shown. The panels from left to right correspond to the case for $i = \Theta = 30°$, 45°, 60°, and 90°. For $i = \Theta = 90°$, the time when the observed flux becomes 0 depends on $\Delta\psi$, which is shown by the filled circle, filled diamond, filled square, and filled triangle for $\Delta\psi = 5°$, 10°, 30°, and 50° in the rightmost lower panel.

pointlike approximation. From this figure, we observe (unsurprisingly) that the deviation from the result calculated using the pointlike approximation increases as the spot area increases. In particular, the deviation becomes significant when the hot spot approaches the invisible zone. This happens because even if the center of the hot spot enters the invisible zone, a part of it may still lay within the visible region. Thus, *when* exactly the flux is going to vanish completely depends strongly on the spot size, as shown in the rightmost lower panel of Fig. 6. On the other hand, we also find that the light curves of hot spots with angular radius up to $\Delta\psi \leq 5°$ are captured by the pointlike approximation within 1% accuracy, if the center of the hot spot lies outside the invisible zone.

In Fig. 7 we show the spot area S outside the invisible zone, normalized by R^2. We can see that when $i = \Theta$ and $\Delta\psi$ are large, a portion of the hot spot's area enters the invisible zone earlier over the course of the star's rotation. We also observe that the spot area normalized by R^2 becomes constant with $\Delta\psi = 70°$ and $i = \Theta = 90°$ for $t/T \sim 0.45$–0.5, where the invisible zone completely enters into the hot spot. This happens due to the following. When the hot spot has a large opening angle, $\Delta\psi$, it is more difficult for it to be completely eclipsed (i.e., to fall completely in the invisible zone). Notice that the opening angle of the invisible zone is given by

$$\Delta\psi_{\rm cri} \equiv \pi - \psi_{\rm cri}, \tag{22}$$

and it decreases as the compactness increases. Consequently, if the opening angle of the spot $\Delta\psi$ is larger than $\Delta\psi_{\rm cri}$, a fraction of the hot spot is always visible.

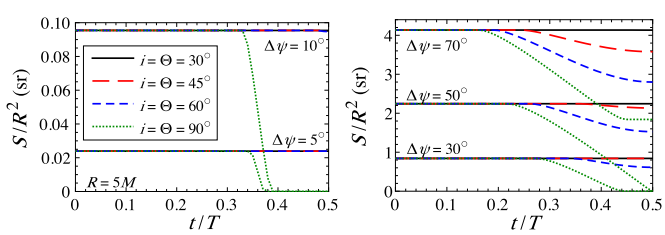

FIG. 7. The visible area of the hot spot (normalized by R^2) for the neutron star model with $R = 5M$, for various combinations of $\Delta\psi$ and $i = \Theta$. The significant decrease in the visible area indicates when a part of the hot spot enters the invisible zone. When $\Delta\psi = 70°$, the visible hot area never drops to 0 regardless of the values of $i = \Theta$ considered.

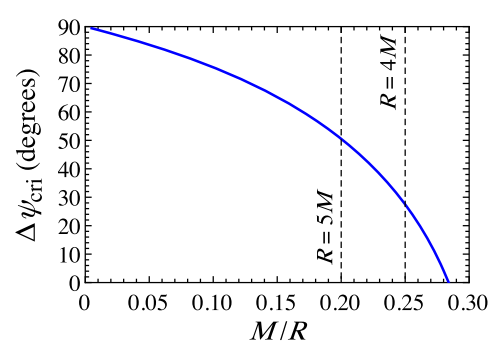

FIG. 8. The critical value of the opening angle, $\Delta\psi_{\rm cri}$, given by $\Delta\psi_{\rm cri} = \pi - \psi_{\rm cri}$ is shown as a function of M/R. For the case when the opening angle $\Delta\psi$ is larger than $\Delta\psi_{\rm cri}$ (the region above the line) the hot spot cannot entirely enter into the invisible zone. Two vertical dashed lines correspond to the values of M/R for the stellar models with $R = 5M$ and $4M$.

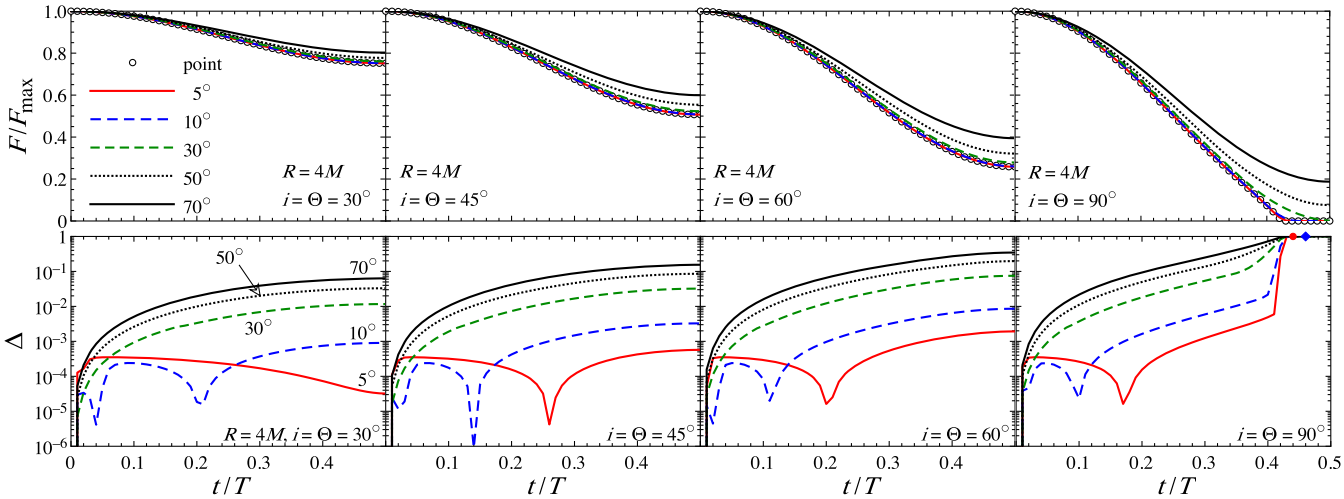

FIG. 9. Same as Fig. 6, but for the neutron star model with $R = 4M$.

In Fig. 8, we show the value of $\Delta\psi_{\rm cri}$ as a function of M/R, where the two vertical dashed lines correspond to the two stellar models with $R = 5M$ (left line) and $4M$ (right line). The values of $\Delta\psi_{\rm cri}$ are respectively 50.6° and 27.4° for stars with radii $R = 5M$ and $R = 4M$. Hence, in Figs. 6 and 7, we can understand that the hot spot with $\Delta\psi = 70°$ is always visible. Moreover, we see that, in principle, one could constrain the relation between the stellar compactness and the opening angle of hot spot. Specifically, if the flux vanishes (i.e., the hot spot entirely enters into the invisible zone) one can constrain the size of the opening angle of the hot spot to be in the region below the line in Fig. 8.

Similarly, we also calculated the light curves for the neutron star model with $R = 4M$, for which $\psi_{\rm cri}$ is larger in comparison to the previous case ($R = 5M$); i.e., the invisible zone becomes smaller. In Fig. 9, we show the light curves taking into account the finite size of the hot spot together with the results using the pointlike approximation in the upper panels. The relative deviation [calculated using Eq. (21)] is shown in the lower panels. The qualitative behavior of the light curve for $R = 4M$ is very similar to that for $R = 5M$. However, since the invisible zone is now smaller, the hot spot area hardly enters it. In fact, since $\Delta\psi_{\rm cri} = 27.4°$, even a relatively small hot spot with $\Delta\psi = 30°$ is always visible when $i = \Theta = 90°$. Finally we see that, even for fairly compact neutron stars, the light curves from a hot spot with $\Delta\psi \leq 5°$ can be well captured using pointlike approximation, with relative errors of less than 1%, if the center of the hot spot is outside the invisible zone.

In Fig. 10, we show the visible hot spot area (again normalized by R^2). We see that due to the smaller size of the invisible zone, it can now completely lay within the hot spot for $\Delta\psi = 30°$, 50°, and 70° when the hot spot is behind the neutron star. When this happens the visible spot area becomes constant.

B. Annular hot spots

Now let us consider a ring-shaped hot spot, as illustrated in the right-hand side of Fig. 5. In particular, we consider hot spots with $\Delta\psi = 35°$ and 70°, while varying the values of $\Delta\psi_i$.

In Fig. 11, we show the light curves from the spot with $\Delta\psi = 70°$ for the neutron star with $R = 5M$ in the upper panels and with $R = 4M$ in the lower panels, where the panels from left to right correspond to the results for $i = \Theta = 30°$, 45°, 60°, and 90°. In each panel we show the light curves for $\Delta\psi_i = 0°$, 10°, 30°, 50°, and 65°, which correspond to $\Delta\psi_i/\Delta\psi = 0$, 0.14, 0.43, 0.71, and 0.93 respectively. That is, the larger the $\Delta\psi_i/\Delta\psi$, the thinner the radiating region of the hot spot. The case of $\Delta\psi_i = 0°$ is shown only as a reference to facilitate the comparison with the circular hot spot case discussed in the previous subsection.

In Fig. 11, we observe that the difference between the minimum flux, $F_{\rm min}$ (at $t/T = 0.5$), and the maximum flux, $F_{\rm max}$ (at $t/T = 0$), decreases as $\Delta\psi_i$ increases in all the cases studied here. Additionally, we see that such a difference becomes larger as the angle of $i = \Theta$ increases. To demonstrate this behavior, we show the value of $(F_{\rm max} - F_{\rm min})/F_{\rm max}$ with various angles of $i = \Theta$ in

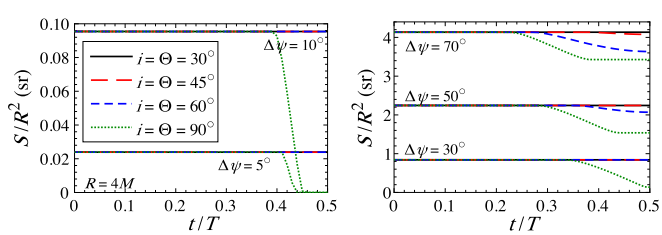

FIG. 10. Same as Fig. 7, but for the neutron star model with $R = 4M$. This more compact neutron star has a smaller invisible zone and therefore hot spot sizes which would become invisible in the $R = 5M$ case ($\Delta\psi = 30°$ and 50°) are now always visible.

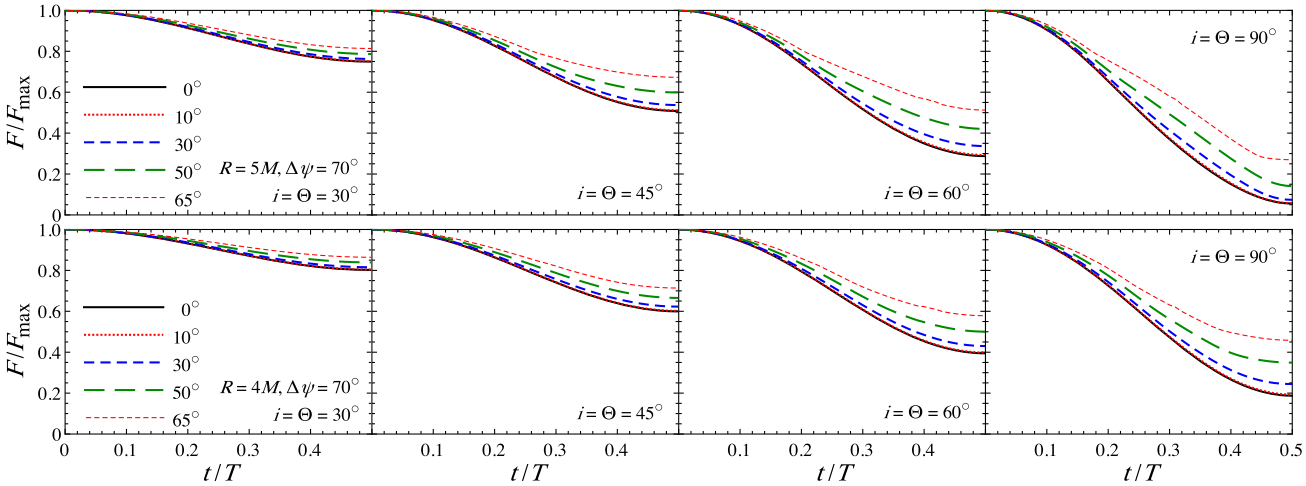

FIG. 11. Light curves from the annular hot spot with $\Delta\psi = 70°$. The upper and lower panels correspond to the observed flux normalized by the maximum flux for the neutron star model with $R = 5M$ and $4M$, respectively. The panels from left to right correspond to the results for $i = \Theta = 30°$, 45°, 60°, and 90°. In each panel, the different lines correspond to the results with different values of $\Delta\psi_i$, i.e., $\Delta\psi_i = 0°$, 10°, 30°, 50°, and 65°.

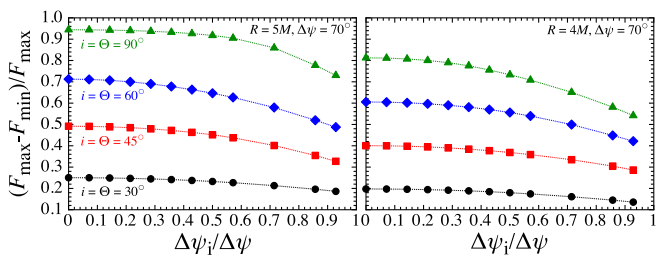

FIG. 12. The ratio of the difference between the maximum and minimum flux to the maximum flux is shown as a function of $\Delta\psi_i/\Delta\psi$ with $\Delta\psi = 70°$, where the circles, squares, diamonds, and triangles correspond to the results for $i = \Theta = 30°$, 45°, 60°, and 90°. The left and right panels correspond to the results for the neutron star model with $R = 5M$ and $4M$.

Fig. 12, where the left and right panels correspond to the results for the neutron star model with $R = 5M$ and $4M$. Furthermore, since it can happen that the invisible zone completely enters into the internal region with the opening angle $\Delta\psi_i$ for the case of $i = \Theta = 90°$, i.e., the hot spot is not eclipsed by the invisible zone when the hot spot approaches the backside of the star, one can see in Fig. 11 that the shape of the light curve can deviate from that predicted by a filled hot spot. This could be used (in principle) to distinguish between the two different hot spot geometries.

In Fig. 13, the light curves from the ring-shaped hot spot with $\Delta\psi = 35°$ are shown for $R = 5M$ (upper panel) and for $R = 4M$ (lower panel). In Fig. 14, we show the value of $(F_{\max} - F_{\min})/F_{\max}$ is as a function of $\Delta\psi_i/\Delta\psi$. Here, we considered $\Delta\psi_i = 0°$, 5°, 15°, 25°, and 33°, which

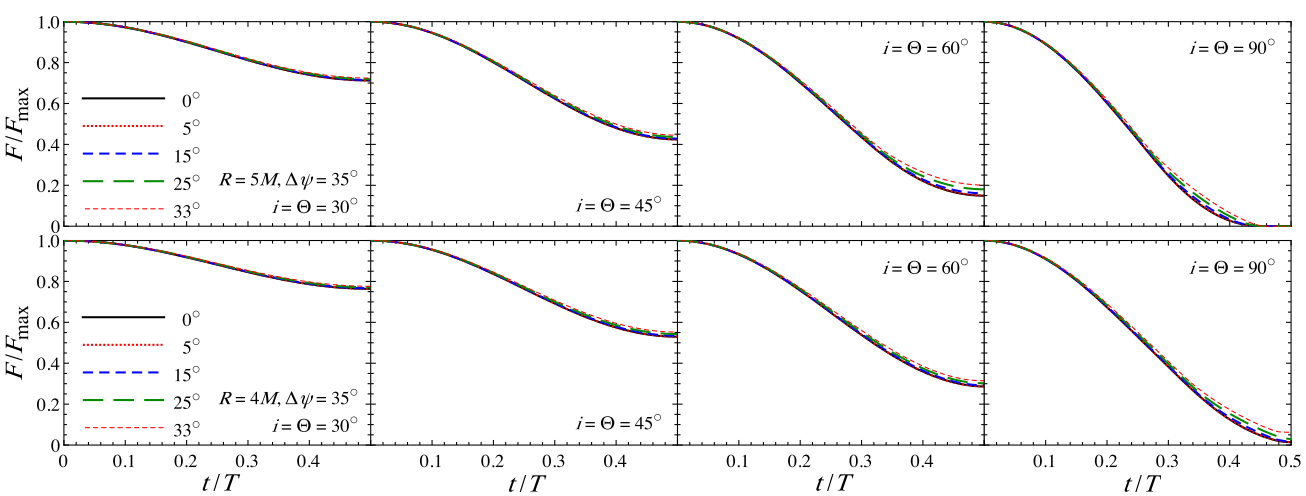

FIG. 13. Same as Fig. 11, but for the neutron star model with $\Delta\psi = 35°$.

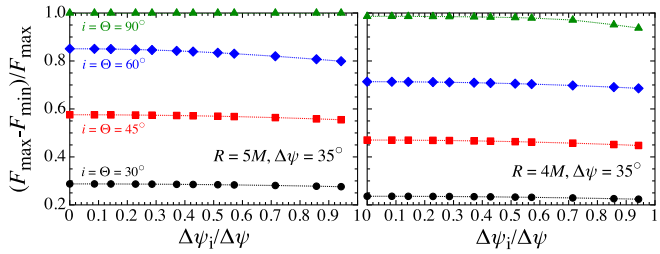

FIG. 14. Same as Fig. 12, but for the neutron star model with $\Delta\psi = 35°$.

correspond to the same values of $\Delta\psi_i/\Delta\psi$ as for the $\Delta\psi = 70°$ case, i.e., $\Delta\psi_i/\Delta\psi = 0$, 0.14, 0.43, 0.71, and 0.93, respectively. The behavior of the light curves is qualitatively the same as in the case with $\Delta\psi = 70°$, but the $\Delta\psi_i$ dependence is quite weak. Nevertheless, since the invisible zone becomes larger as the stellar compactness is smaller, one may have a chance to observe the deviation in the light curve for the less compact stellar models, although such a deviation must be still very small. In practice, for $i = \Theta = 60°$ one can see a stronger dependence on $\Delta\psi_i$ in the light curve for the neutron star model with $R = 5M$ than that from the model with $R = 4M$. Anyway, if $\Delta\psi$ is less than 35°, it seems to be difficult to observationally identify the $\Delta\psi_i$ dependence. In such a case, via the observation of the light curve one may be able to discuss the relation between the stellar compactness and the spot size ($\Delta\psi$) independently of $\Delta\psi_i$.

IV. CONCLUSION

In this work we have calculated bolometric light curves from a single hot spot on a slowly rotating neutron star, taking into account the effects of the size and shape of the spot. In order to explore how the light curves are affected by changes in shape and size, we have specifically considered a filled circle hot spot and a ring-shaped hot spot. We found that the light curve from a filled circle hot spot that has an opening angle of less than 5° can be estimated with good accuracy (less than 1%) even with the pointlike approximation if the center of the hot spot is outside the invisible zone. Moreover, we showed that since the invisible zone at the far side of the star becomes smaller as the stellar compactness increases, the light curves may not be eclipsed if the spot size is large enough for large compactnesses. Thus, through the observation of light curves, one may in principle constrain the relation between the stellar compactness and the spot size (see Fig. 8).

For annular hot spots, we found that the resulting light curves are hardly distinguishable from the filled circular case, when the opening angle of the outer boundary of the hot spot is less than ~35°. This result yields a conservative typical hot spot size for which its geometry does not affect the resulting light curve. This is particularly interesting given the fact that hydromagnetic numerical simulations of accreting flows of matter onto millisecond pulsars indicate that the resulting hot spot is not necessarily circular [43,44] with implications to the modeling of known sources [45,46] as mentioned previously.

In this study, as a first step, we considered the light curve from a slowly rotating neutron star in order to isolate the finite size and geometry influences on the resulting light curves. To bring our work to the level of astrophysical realism necessary to analyze, e.g., real NICER data, it is important to revisit some of our simplifying assumptions. For instance, the inclusion of Doppler and aberration effects due to the star's rotation can affect light curves obtained here by skewing them towards the left (e.g., in Fig. 6) and decreasing their amplitudes. On the other hand, delays in the travel time from photons emitted from different locations within the hot spot are expected to be small, although it would be of interest to investigate this for large hot spots where the inclusion of these two effects will enhance the difference of the resulting light curves relative to those studied here. It would also be interesting to study the inclusion of a second hot spot and (in the case of the annular geometry) allow the excised inner circle to be off center with respect to the outer boundary. These however come at the cost of expanding the parameter space to be studied. For rapidly rotating neutron stars $\omega \gtrsim 1800$ Hz, the inclusion of the rotation induced quadrupolar deformation of the star is critical for light curve modeling [33–35]. Finally, one could describe the radiation emitted using blackbody spectra. The inclusion of additional ingredients and an analysis of how they affect the results presented here will be studied in the future.

ACKNOWLEDGMENTS

H. S. acknowledges support in part by Grant-in-Aid for Scientific Research (C) through Grant No. 17K05458 provided by JSPS. H. O. S. was supported by NASA Grants No. NNX16AB98G and No. 80NSSC17M0041 and thanks Nicolás Yunes for discussions. G. P. acknowledges financial support provided under the European Union's H2020 ERC, Starting Grant No. DarkGRA-757480. We thank Sharon Morsink for bringing Refs. [41,42] to our attention. Part of this work was achieved using the grant of NAOJ Visiting Joint Research supported by the Research Coordination Committee, National Astronomical Observatory of Japan (NAOJ), National Institutes of Natural Sciences (NINS). H. O. S. and G. P. acknowledge the hospitality of the Division of Theoretical Astronomy of NAOJ.

[1] S. L. Shapiro and S. A. Teukolsky, *Black Holes, White Dwarfs, and Neutron Stars: The Physics of Compact Objects* (Wiley-Interscience, New York, 1983).
[2] J. M. Lattimer and M. Prakash, Phys. Rep. **621**, 127 (2016).
[3] P. Demorest, T. Pennucci, S. Ransom, M. Roberts, and J. Hessels, Nature (London) **467**, 1081 (2010).
[4] J. Antoniadis *et al.*, Science **340**, 1233232 (2013).
[5] H. T. Cromartie *et al.*, arXiv:1904.06759.
[6] B. P. Abbott *et al.* (LIGO Scientific and Virgo Collaboration), Phys. Rev. Lett. **119**, 161101 (2017).
[7] B. P. Abbott *et al.* (LIGO Scientific and Virgo Collaboration), Phys. Rev. Lett. **121**, 161101 (2018).
[8] B. Kumar and P. Landry, Phys. Rev. D **99**, 123026 (2019).
[9] E. Annala, T. Gorda, A. Kurkela, and A. Vuorinen, Phys. Rev. Lett. **120**, 172703 (2018).
[10] F. Özel and P. Freire, Annu. Rev. Astron. Astrophys. **54**, 401 (2016).
[11] A. L. Watts *et al.*, Rev. Mod. Phys. **88**, 021001 (2016).
[12] A. L. Watts, W. F. Yu, J. Poutanen, S. Zhang, S. Bhattacharyya, S. Bogdanov, and L. Ji, Sci. China Phys. Mech. Astron. **62**, 29503 (2019).
[13] A. L. Watts, AIP Conf. Proc. **2127**, 020008 (2019).
[14] L. R. Weih, E. R. Most, and L. Rezzolla, arXiv:1905.04900.
[15] K. C. Gendreau, Z. Arzoumanian, and T. Okajima, Proc. SPIE Int. Soc. Opt. Eng. **8443**, 844313 (2012).
[16] Z. Arzoumanian *et al.*, Proc. SPIE Int. Soc. Opt. Eng. **9144**, 914420 (2014).
[17] K. Gendreau and Z. Arzoumanian, Nat. Astron. **1**, 895 (2017).
[18] K. H. Lo, M. Coleman Miller, S. Bhattacharyya, and F. K. Lamb, Astrophys. J. **776**, 19 (2013).
[19] K. H. Lo, M. C. Miller, S. Bhattacharyya, and F. K. Lamb, Astrophys. J. **854**, 187 (2018).
[20] M. C. Miller and F. K. Lamb, Astrophys. J. **808**, 31 (2015).
[21] D. Psaltis, F. Özel, and D. Chakrabarty, Astrophys. J. **787**, 136 (2014).
[22] M. C. Miller, Astrophys. J. **822**, 27 (2016).
[23] S. Bogdanov, Eur. Phys. J. A **52**, 37 (2016).
[24] K. R. Pechenick, C. Ftaclas, and J. M. Cohen, Astrophys. J. **274**, 846 (1983).
[25] D. A. Leahy and L. Li, Mon. Not. R. Astron. Soc. **277**, 1177 (1995).
[26] M. C. Miller and F. K. Lamb, Astrophys. J. **499**, L37 (1998).
[27] A. M. Beloborodov, Astrophys. J. **566**, L85 (2002).
[28] J. Poutanen, AIP Conf. Proc. **1068**, 77 (2008).
[29] J. Poutanen and M. Gierlinski, Mon. Not. R. Astron. Soc. **343**, 1301 (2003).
[30] J. Poutanen and A. M. Beloborodov, Mon. Not. R. Astron. Soc. **373**, 836 (2006).
[31] H. Sotani and U. Miyamoto, Phys. Rev. D **98**, 103019 (2018).
[32] D. Psaltis and F. Özel, Astrophys. J. **792**, 87 (2014).
[33] C. Cadeau, D. A. Leahy, and S. M. Morsink, Astrophys. J. **618**, 451 (2005).
[34] C. Cadeau, S. M. Morsink, D. Leahy, and S. S. Campbell, Astrophys. J. **654**, 458 (2007).
[35] S. M. Morsink, D. A. Leahy, C. Cadeau, and J. Braga, Astrophys. J. **663**, 1244 (2007).
[36] J. Nättilä and P. Pihajoki, Astron. Astrophys. **615**, A50 (2018).
[37] H. Sotani and U. Miyamoto, Phys. Rev. D **96**, 104018 (2017).
[38] H. Sotani, Phys. Rev. D **96**, 104010 (2017).
[39] H. O. Silva and N. Yunes, Phys. Rev. D **99**, 044034 (2019).
[40] H. O. Silva and N. Yunes, arXiv:1902.10269.
[41] M. Baubock, D. Psaltis, and F. Ozel, Astrophys. J. **811**, 144 (2015).
[42] W. Lockhart, S. E. Gralla, F. Özel, and D. Psaltis, arXiv:1904.11534.
[43] A. K. Kulkarni and M. M. Romanova, Astrophys. J. **633**, 349 (2005).
[44] A. K. Kulkarni and M. M. Romanova, Mon. Not. R. Astron. Soc. **433**, 3048 (2013).
[45] A. Ibragimov and J. Poutanen, Mon. Not. R. Astron. Soc. **400**, 492 (2009).
[46] J. J. E. Kajava, A. Ibragimov, M. Annala, A. Patruno, and J. Poutanen, Mon. Not. R. Astron. Soc. **417**, 1454 (2011).
[47] H. Sotani and U. Miyamoto, Phys. Rev. D **98**, 044017 (2018).
[48] V. E. Zavlin, G. G. Pavlov, and Yu. A. Shibanov, Astron. Astrophys. **315**, 141 (1996).
[49] C. O. Heinke, G. B. Rybicki, R. Narayan, and J. E. Grindlay, Astrophys. J. **644**, 1090 (2006).
[50] C. B. Haakonsen, M. L. Turner, N. A. Tacik, and R. E. Rutledge, Astrophys. J. **749**, 52 (2012).
[51] T. Salmi, V. Suleimanov, and J. Poutanen, Astron. Astrophys. **627**, A39 (2019).